Probabilities of polar aligned disks in binary star systems

Ted Johnson,[1,2] Rebecca G. Martin,[1,2] Stephen Lepp,[1,2] and Stephen H. Lubow[3]

[1]*Nevada Center for Astrophysics, University of Nevada, Las Vegas, 4505 South Maryland Parkway, Las Vegas, NV 89154, USA*
[2]*Department of Physics and Astronomy, University of Nevada, Las Vegas, 4505 South Maryland Parkway, Las Vegas, NV 89154, USA*
[3]*Space Telescope Science Institute, 3700 San Martin Drive, Baltimore, MD 21218, USA*

ABSTRACT

Circumbinary gas disks that are misaligned to the binary orbital plane evolve toward either a coplanar or a polar-aligned configuration with respect to the binary host. The preferred alignment can be found analytically in the limit of a massless disk, however disk-binary interactions make the massive disk case much more challenging. We employ the N-body code REBOUND to investigate the dynamics of 3-body systems and use Monte Carlo methods to quantify the probabilities of each alignment for an initially randomly orientated disk around a given system.

1. INTRODUCTION

Observed circumbinary planets – those orbiting around two stars – have been mostly found to orbit in the same plane as their hosts (Doyle et al. 2011; Orosz et al. 2012; Welsh et al. 2012). However, this is likely a result of selection effects (citations by David Martin..). Misaligned disks around eccentric binaries evolve either to coplanar (citations) to a polar state (Aly et al. 2015; Martin & Lubow 2017). A polar-aligned debris disk has been found in the 99 Her system (Kennedy et al. 2012) and polar-aligned gas disks have been found in the HD 98800 (Kennedy et al. 2019) and V773 Tau systems (Kenworthy et al. 2022). AC Her, a post-AGB system with a polar-inclined disk, may host the first circumbinary planet found in a polar orbit (**??**Martin et al. 2023).

The alignment of circumbinary planets, and the alignment of the disks from which they form, are determined by their interaction history with their host stars. For a massless circumbinary disk, the type of nodal precession can be split into two categories:

1. **Precession about the angular momentum vector of the binary.** In the case where the planet/disk is slightly misalignend, its own angular momentum vector precesses about that of the binary (e.g., Bate et al. 2000; Lubow & Ogilvie 2000). This is characterized by near constant inclination and oscillation of the longitude of the ascending node. Included in this case is the sub-classification of retrograde orbits (those whose angular momentum vectors are misaligend by $\sim$ 180 deg) and the two trivial cases of perfectly aligned/misaligend orbits which do not precess.

2. **Libration about the eccentricity vector of the binary.** In the case where misalignment is high (i.e. near perpendicular) the angular momentum vector of the planet/disk precesses about the eccentricity vector of the binary (e.g., Verrier & Evans 2009; Farago & Laskar 2010; Doolin & Blundell 2011). This is called a librating orbit. In this case the mutual inclination of the disk oscillates about the polar configuration.

However, for a massive disk, there are additional types of nodal precesion.... (describe) (Abod et al. 2022).

Planets form with the orbital characteristics given by their progenitor disks (e.g., Childs & Martin 2021), so it is sufficient in this work to discuss disk dynamics only. Differential precession between adjacent annular regions in a disk cause dissipation, ultimately dampening precession or libration so that the disk reaches a steady state on its viscous timescale (Bate et al. 2000, see also Nixon et al. (2011); Foucart & Lai (2013, 2014)). Therefore, it is appropriate to map a disk's initial interactions with a binary (prograde precession, libration, retrograde precession) to the disk's final configuration (prograde coplanar, circumpolar, retrograde coplanar, respectively).

In the case of a massless disk, the type of interaction can be determined analytically from just the binary eccentricity and the direction of the disk's specific angular momentum vector (parameterized by the disk inclination and its longitude of the ascending node Zanazzi & Lai 2018). Given priors on these quantities we can predict the observed frequencies of circumbinary disks (and planets) in the polar configuration. Ceppi et al. (2024) do just this – finding the fractions of binaries with polar

disks and the mean eccentricities of those binaries as a function of two free parameters.

In this work we will study the more general case of a massive disk. The resulting polar frequency function only contains one additional parameter, but the orbital parameters of the binary can now change due to interactions with the disk. The additional complications of this case require the application of numerical simulations; we use the N-body code REBOUND (Rein & Liu 2012) to simulate the dynamics of a three-body system, with a massive point particle used as a stand-in for the disk. Abod et al. (2022) found that this 3-body setup is a valid description of a disk with angular momentum equal to that of the third body in the limit that the disk mass does not change (i.e. no accretion). This setup also cannot account for warping effects and disk breakage as we must treat the disk as a solid body. We describe this setup in detail in Section 2

[describe the regime we are working in]

2. METHODS

We describe two methods to approximate the evolution of a binary-disk system, each optimized for a different balance of computational cost and physical realism. First, we use the N-body code REBOUND (Rein & Liu 2012) to simulate the disk using a point mass. The second method employs a Runge-Kutta-Fehlburg integrator to solve equations (7-10) from Martin & Lubow (2019). These equations treat the central binary in the quadrupole approximation, but can be solved extremely efficiently. The code used to run these simulations is publically available[1].

2.1. *Geometric considerations*

The dynamical state of the disk (i.e. prograde circulation, libration, etc.) is determined by tracking two relevant orbital elements: mutual inclination i and longitude of ascending node Ω. Each simulation method gives as an output the direction of the disk angular momentum relative to the binary $\boldsymbol{l}$. We define a coordinate system relative to the binary, with the z-axis to be along the angular momentum vector, the x-axis to be along the eccentricity vector, and the y-axis so that the coordinate system is right-handed.

The relevant coordinates are then defined

$$\cos i = \frac{\boldsymbol{l} \cdot \hat{\boldsymbol{z}}}{\|\boldsymbol{l}\|} \qquad (1)$$

and

---

[1] https://github.com/tedjohnson12/misaligned__cb__disk
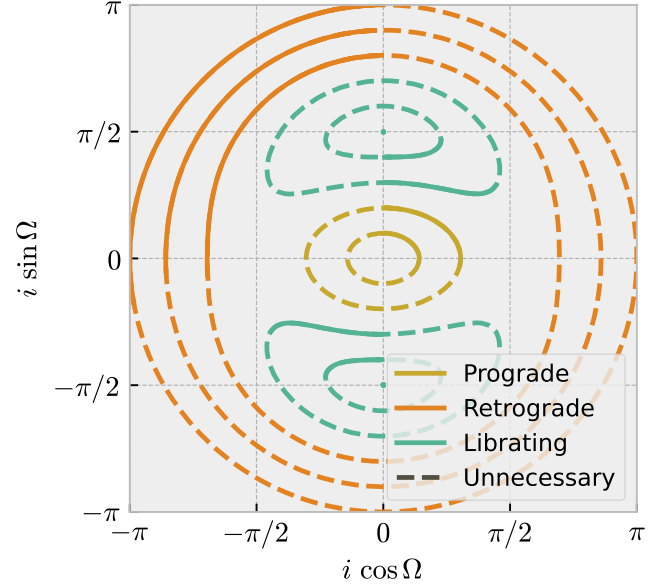
Figure 1. Example of system simulation and state determination. This figure tracks the orbital parameters of a massless third body orbiting a $1 M_\odot$ binary with equal mass stars and $e_b = 0.4$. Initially $\Omega = \frac{\pi}{2}$. Solid lines indicate the portion of the simulation that is required to determine the state. Dashed lines complete the evolution back to the system's initial conditions but are not needed for our analysis. In general, we will only integrate until the state of the system can be determined.

$$\Omega = \arctan2(\boldsymbol{l} \cdot \hat{\boldsymbol{x}}, -\boldsymbol{l} \cdot \hat{\boldsymbol{y}}) \qquad (2)$$

Given some initial (i, Ω), the system can be evolved forward in time to recover the familiar diagram shown in Figure 1. cite papers that have similar figures. This visualiztaion also allows the dynamical state to be resolved programically, as a librating state will repeatedly cross the y-axis and never cross the x-axis, and a circulating state will sequentially cross each axis in an order that can determine if it is prograde or retrograde.

2.2. *Using* REBOUND

We use REBOUND's Python interface to initialize our simulation. Table 1 describes the simulation's input parameters. We integrate the system using the IAS15 15th order Gauss-Radau integrator (Rein & Spiegel 2015) until we can determine the system's state.

Not much can be learned from a single simulation as it only allows us to map from one point in (i, Ω) space to an end state. To infer the behavior of a population (and from that compute a polar fraction) we employ a Monte Carlo (MC) method, sampling isotropically on the (i, Ω)

name	symbol	type	description
mass_binary	M_b	float	The total mass of the binary in solar masses.
mass_fraction	f_b	float	The ratio between the secondary mass and the binary mass M_2/M_b.
semimajor_axis_binary	a_b	float	The semimajor axis of the binary orbit.
eccentricity_binary	e_b	float	The eccentricity of the binary orbit.
mass_planet	m_p	float	The mass of the third body.
semimajor_axis_planet	a_p	float	The semimajor of the third body orbiting the binary center of mass.
inclination_planet	i	float	The mutual inclination of the binary and the third body.
lon_ascending_node_planet	Ω	float	The longitude of the ascending node of the third body.
true_anomaly_planet	ν	float	The true anomaly of the third body.
gr	-	bool	Whether to include effects from general relativity.
eccentricity_planet	e_p	float	The eccentricity of the third body's orbit.
arg_pariapsis_planet	ω	float	The argument of pariapsis of the third body's orbit.

Table 1. REBOUND Simulation parameters

sphere. That is, $\Omega \in \mathcal{U}(0, 2\pi)$ and $i \in \{\arcsin(2u-1) + \frac{\pi}{2} \mid u \in \mathcal{U}(0,1)\}$.

Each MC run is initialized with the conditions of the binary as well as the angular momentum of the disk. We then sample i and Ω in batches of four simulations, using a bootstrap metric after each batch to compute the polar fraction. Sampling stops when the bootstrap-computed confidence interval reaches a prescribed value. A typical simulation takes on the order of $0.1-1$ s, so we save the results of each simulation in an SQLite database between batches. When an MC sampler is initialized it queries this database for all relevant passed simulations, ingests them, and only runs new simulations if a more stringent confidence interval is requested.

2.3. *Runge-Kutta-Fehlburg method*

In addition to using REBOUND in Section 2.2 we can solve the same problem using a slightly more analytical approach. Martin & Lubow (2019) found a set of first-order differential equations (their Equations 7-10) based on previous work by Farago & Laskar (2010) that describes the coupled behavior of the disk angular momentum direction and the binary eccentricity. We solve these equations using the Runge-Kutta-Fehlberg (RKF) method ref? – a numerical method similar to the common 4th order Runge-Kutta integrator, but that computes a 5th order solution to allow for a variable step

size. The cost of this method is that it treats the binary in the quadrupole approximation, meaning we are not sensitive to the effects of the binary mass fraction, but the computational cost is extremely low; we are able to run 10^4-10^5 simulations per second – about 10,000 times faster than REBOUND.

The added computational efficiency means this method is not restricted to an MC method with hundreds of samples; we can compute a grid of $\sim 10^6$ in less than a minute to get a very accurate measure of the polar fraction.

3. RESULTS

4. DISCUSSION
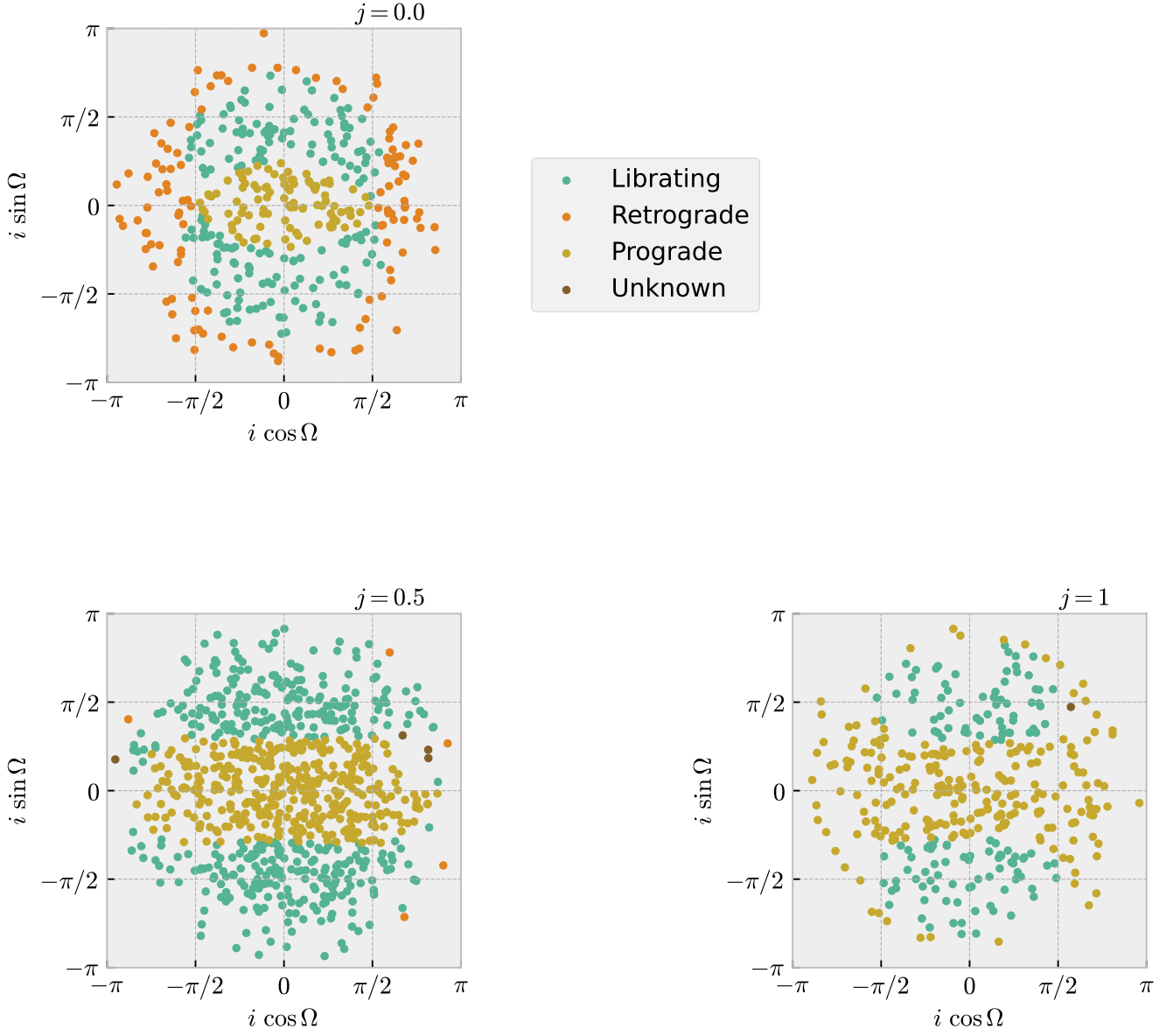
5. CONCLUSIONS

6. ACKNOWLEDGEMENTS

REFERENCES

Abod, C. P., Chen, C., Smallwood, J., et al. 2022, Monthly Notices of the Royal Astronomical Society, 517, 732, doi: 10.1093/mnras/stac2601

[2] https://github.com/tedjohnson12/bin-disk-paper

Figure 2. Monte Carlo results for a $1M_\odot$ equal mass binary with $e_b = 0.4$ for $j = 0, 0.5, 1$. The position of each point shows the initial condition of the simulation, and the color denotes the dynamical state. Note that some are marked as "unknown". This is because we set a 1000 orbit limit on the integration for the sake of computational time.

Aly, H., Dehnen, W., Nixon, C., & King, A. 2015, Monthly Notices of the Royal Astronomical Society, 449, 65, doi: 10.1093/mnras/stv128

Bate, M. R., Bonnell, I. A., Clarke, C. J., et al. 2000, Monthly Notices of the Royal Astronomical Society, 317, 773, doi: 10.1046/j.1365-8711.2000.03648.x

Ceppi, S., Cuello, N., Lodato, G., et al. 2024, Astronomy and Astrophysics, 682, A104, doi: 10.1051/0004-6361/202348375

Childs, A. C., & Martin, R. G. 2021, The Astrophysical Journal, 920, L8, doi: 10.3847/2041-8213/ac2957
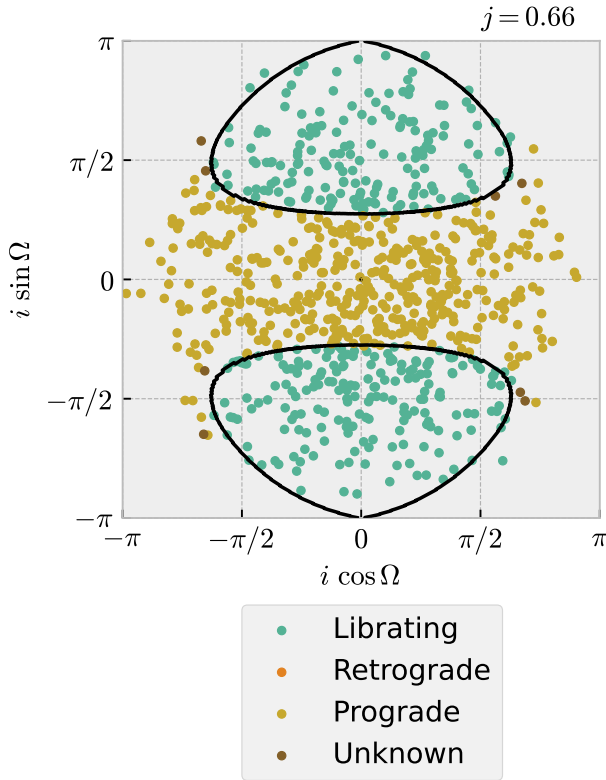
Figure 3. Contour lines denoting solution boundaries found via the RKF method compared to MC results of the same conditions. Binary setup is the same as in Figure 2, but for $j = 0.66$, which is its critical value (see Martin & Lubow 2019; Abod et al. 2022). The grid here includes 250,000 points. There is some disagreement between RKF and RE-BOUND, which we attribute to misclassification due to behavior on the orbital timescale (i.e. small variations in Ω that cause the simulation to temporarily cross the y-axis twice, giving the false appearance of libration). We can fix this

Doolin, S., & Blundell, K. M. 2011, Monthly Notices of the Royal Astronomical Society, 418, 2656, doi: 10.1111/j.1365-2966.2011.19657.x

Doyle, L. R., Carter, J. A., Fabrycky, D. C., et al. 2011, Science, 333, 1602, doi: 10.1126/science.1210923

Farago, F., & Laskar, J. 2010, Monthly Notices of the Royal Astronomical Society, 401, 1189, doi: 10.1111/j.1365-2966.2009.15711.x

Foucart, F., & Lai, D. 2013, The Astrophysical Journal, 764, 106, doi: 10.1088/0004-637X/764/1/106

—. 2014, Monthly Notices of the Royal Astronomical Society, 445, 1731, doi: 10.1093/mnras/stu1869

Kennedy, G. M., Wyatt, M. C., Sibthorpe, B., et al. 2012, Monthly Notices of the Royal Astronomical Society, 421, 2264, doi: 10.1111/j.1365-2966.2012.20448.x

Kennedy, G. M., Matrà, L., Facchini, S., et al. 2019, Nature Astronomy, 3, 230, doi: 10.1038/s41550-018-0667-x

Kenworthy, M. A., González Picos, D., Elizondo, E., et al. 2022, Astronomy and Astrophysics, 666, A61, doi: 10.1051/0004-6361/202243441

Lubow, S. H., & Ogilvie, G. I. 2000, The Astrophysical Journal, 538, 326, doi: 10.1086/309101

Luger, R., Bedell, M., Foreman-Mackey, D., et al. 2021, Mapping Stellar Surfaces III: An Efficient, Scalable, and Open-Source Doppler Imaging Model, doi: 10.48550/arXiv.2110.06271

Martin, R. G., & Lubow, S. H. 2017, The Astrophysical Journal, 835, L28, doi: 10.3847/2041-8213/835/2/L28

—. 2019, Monthly Notices of the Royal Astronomical Society, 490, 1332, doi: 10.1093/mnras/stz2670

Martin, R. G., Lubow, S. H., Vallet, D., Anugu, N., & Gies, D. R. 2023, The Astrophysical Journal, 957, L28, doi: 10.3847/2041-8213/ad0730

Nixon, C. J., King, A. R., & Pringle, J. E. 2011, Monthly Notices of the Royal Astronomical Society, 417, L66, doi: 10.1111/j.1745-3933.2011.01121.x

Orosz, J. A., Welsh, W. F., Carter, J. A., et al. 2012, The Astrophysical Journal, 758, 87, doi: 10.1088/0004-637X/758/2/87

Rein, H., & Liu, S. F. 2012, A&A, 537, A128, doi: 10.1051/0004-6361/201118085

Rein, H., & Spiegel, D. S. 2015, MNRAS, 446, 1424, doi: 10.1093/mnras/stu2164

Verrier, P. E., & Evans, N. W. 2009, Monthly Notices of the Royal Astronomical Society, 394, 1721, doi: 10.1111/j.1365-2966.2009.14446.x

Welsh, W. F., Orosz, J. A., Carter, J. A., et al. 2012, Nature, 481, 475, doi: 10.1038/nature10768

Zanazzi, J. J., & Lai, D. 2018, Monthly Notices of the Royal Astronomical Society, 473, 603, doi: 10.1093/mnras/stx2375